# Tuning Photoinduced Electron Transfer in POM-bodipy Hybrids by Controlling the Environment; Experiment and Theory.

Georgios Toupalas,[a] Joshua Karlsson,[b] Fiona A. Black,[b] Albert Masip-Sánchez,[c] Xavier López,[c] Youssef Ben M'Barek,[a] Sébastien Blanchard,[a] Anna Proust,[a] Sandra Alves,[a] Pavel Chabera,[d] Ian P. Clark,[e] Tönu Pullerits,[d] Josep M. Poblet,[c]* Elizabeth A. Gibson,[b]* Guillaume Izzet[a]*

[a] Sorbonne Université, CNRS, Institut Parisien de Chimie Moléculaire, IPCM, 4 Place Jussieu, F-75005 Paris, France. E-mail: guillaume.izzet@sorbonne-universite.fr ORCID 0000-0002-9849-4939
[b] Energy Materials Laboratory, Chemistry, School of Natural and Environmental Sciences, Newcastle University, Newcastle upon Tyne, NE1 7RU, United Kingdom. E-mail: Elizabeth.gibson@ncl.ac.uk ORCID 0000-0002-6032-343X
[c] Department de Química Física i Inorgànica, Universitat Rovira i Virgili, Marcellí Domingo 1, 43007 Tarragona, Spain. E-mail : josepmaria.poblet@urv.cat ORCID 0000-0002-4533-0623
[d] Chemical Physics and NanoLund, Lund University, Box 124, 22241, Lund, Sweden. E-mail: Tonu.Pullerits@chemphys.lu.se
[e] Central Laser Facility, Research Complex at Harwell, Science and Technology Facilities Council, Rutherford Appleton Laboratory, Harwell Campus, Didcot, Oxfordshire, OX11 0QX, UK. E-mail: ian.p.clark@stfc.ac.uk

**Abstract:** The optical and electrochemical properties of a series of polyoxometalates (POMs) oxoclusters decorated with two bodipy (boron-dipyrromethene) light harvesting units were examined. We evaluated in this polyanionic donor-acceptor system the effect of the solvent and associated counterions on the intramolecular photoinduced electron transfer. Our results show that both solvents and counterions have a major impact upon the energy of the charge transfer state by modifying the solvation shell around the POM. This leads to a significantly shorter charge separation time in case of smaller counterion and slower charge recombination in a less polar solvent. We rationalize these results in terms of Marcus theory and show that solvent and counterion both affect the driving force for photoinduced electron transfer and the reorganization energy. This was corroborated with theoretical investigations combining DFT and molecular dynamics simulations.

## Introduction

Polyoxometalates (POMs) are a class of discrete metal-oxo clusters that display a wide range of chemical properties, often showing promise as building units for multi-functional materials on account of their rich redox chemistry.[1] An important feature of most POMs is their ability to be reduced with several electrons under minor structural rearrangements and the activity of their reduced species in the hydrogen evolution reaction. Consequently POMs are currently drawing a growing attention in the field of (solar) energy conversion for artificial photosynthesis,[2] dye sensitized solar cells[3] and electrochemical energy storage.[4] Despite the surge in research into the use of POMs for energy applications, fundamental insights regarding the electron transfer kinetics in such charged species are scarce. For instance, the effects of solvent and the associated counterions[5] on their reorganization energy remain largely unexplored, the only experimental studies being yet limited to outer-sphere chemical and electrochemical reduction of POMs.[6] An attractive route towards multi-electron photocatalysis is to associate the POM oxocluster to a suitable chromophore sensitizer. Some hybrid systems, in which organic or inorganic dyes are used to stimulate electron transfer to a POM, have been proposed in the past. These have been bound either by electrostatic interactions or covalently by means of an anchoring group.[7] The advantage of a covalently coupled hybrid comes from possessing greater control over the distance and geometry of donor-acceptor moieties, both of which are crucial for modifying the rate of photoinduced electron transfer and understanding photosynthetic energy conversion reactions.[8]

We recently reported the synthesis and photophysical properties of a series of photoactive hybrids based on Keggin-type POMs covalently grafted to bodipy photosensitizers.[9] In these POM-bodipy conjugates, we observed that the occurrence and kinetics of photoinduced electron transfer was strongly dependent on the redox properties of both POM and bodipy units. In this series of compounds, the hybrid displaying the best electron accepting properties, *i.e.* an organosilyl POM derivative, promoted very rapid charge separation ($\tau$=54 ps) upon the excitation of the bodipy unit. Following this work, we wanted to use our model donor-acceptor system to evaluate the effect of the solvent and associated counterion on the intramolecular charge separation kinetics. We decided to examine a Dawson-type hybrid analogue since this platform displays lower electron accepting properties owing to a higher charge than that of the Keggin. Consequently, based on our previous studies on photosensitized POMs,[2b, 7h] it is expected that the Dawson-based system would be slower compared to the Keggin one (both for charge separation and recombination), and therefore more prone to variation upon solvent or counterion change.

Here we report the synthesis of a Dawson-bodipy hybrid, which has been isolated with counterions of different bulkiness - tetrabutyl ammonium (TBA), tetraethyl ammonium (TEA) and tetramethyl ammonium (TMA). The photophysical properties of these Dawson-type hybrids and the previously reported Keggin analogue are examined by changing the solvent and counterion. This information is used to construct a qualitative model of how photoinduced electron transfer is tuned through the control of the reorganization energy in a POM-sensitizer hybrid.

## Results and discussion

### Synthesis

The POM-based building block $(TBA)_6[P_2W_{17}O_{61}\{O(Si-$

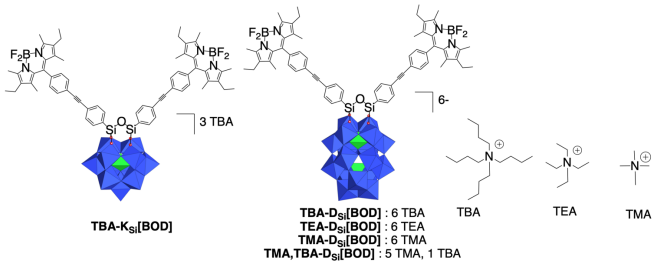


**Scheme 1.** Molecular representations of the POM-based hybrids compounds described in this study. In the polyhedral representation, the $WO_6$ octahedra are depicted with oxygen atoms at the vertices and metal cations buried inside. Color code: $WO_6$ octahedra, blue; $PO_4$ tetrahedra, green.

$C_{31}H_{30}N_2BF_2)_2$}], isolated as a TBA salt, denoted **TBA-D$_{Si}$[BOD]**[10] contains two bodipy units connected to the monolacunary site of a Dawson-type α$_2$-[$P_2W_{17}O_{61}$]$^{10-}$ through a Si-O-Si anchor. Its synthesis was performed in one step from the iodo-aryl terminated POM-based platform by adapting our previously reported procedure involving a Sonogashira cross-coupling reaction.[11] The TBA counterion of the hybrid was modified through precipitation in the presence of TEABr in acetonitrile (MeCN), or TMABr in ethanol (EtOH), after full solubilization of the hybrid in MeCN or dimethylformamide (DMF). Two successive steps of solubilization / precipitation were necessary to achieve a full exchange of the tetra alkyl ammonium salts to give **TEA-D$_{Si}$[BOD]** and **TMA-D$_{Si}$[BOD]**. The last hybrid was poorly soluble in MeCN and fully insoluble in dichloromethane ($CH_2Cl_2$). A single precipitation with TMABr (in EtOH) lead to the compound **TMA,TBA-D$_{Si}$[BOD]**, which contained a mixture of counterions with a stoichiometry TMA/TBA (5/1) and was slightly soluble in $CH_2Cl_2$ (Scheme 1). All the hybrids were characterized by $^1$H, $^{31}$P, $^{11}$B and $^{19}$F NMR spectroscopy, mass spectrometry, elemental analysis, and FT-IR spectroscopy (Figures S1-S5).

## Electrochemistry

The redox properties of **TBA-D$_{Si}$[BOD]** and **TBA-K$_{Si}$[BOD]** were investigated by cyclic voltammetry in $CH_2Cl_2$, MeCN or DMF with tetrabutylammonium hexafluorophosphate ($TBAPF_6$, 0.1 M) as the supporting electrolyte in a standard three-electrode cell, composed of a glassy carbon working electrode, a platinum counter electrode, and a saturated calomel reference electrode (SCE). We also used tetraethylammonium perchlorate ($TEAClO_4$, 0.1 M) and tetramethylammonium tetrafluoroborate ($TMABF_4$, 0.1 M) as supporting electrolytes (Figure S6) to evaluate the effect of the counterion on the redox properties of the Dawson-bodipy hybrid. The redox behavior of all hybrids was similar to those of the parent hybrid platforms, for which the redox properties have previously been reported and discussed.[7g, 7h, 11a, 12] In the reduction part, **TBA-K$_{Si}$[BOD]** and **TBA-D$_{Si}$[BOD]** display reversible reduction waves that correspond to monoelectronic processes located at the tungstic framework (blue dots on Figure S6) followed by simultaneous reduction of both bodipy units (red dots on Figure S6). In the oxidative part, **TBA-K$_{Si}$[BOD]** and **TBA-D$_{Si}$[BOD]** both display a redox process around 1.0 V vs SCE, attributed to the oxidation of the bodipy units. While partial electrochemical reversibility can be observed on this wave in $CH_2Cl_2$ and MeCN (the shape of the oxidation waves is however characteristic of adsorption/redissolution of the oxidized species at the working electrode, which slighlty lowers the precision of this measurement),[13] it is fully irreversible in DMF. As can be seen from the cyclic voltammograms, the redox properties of all hybrids are significantly affected by the modification of the solvent and/or electrolyte. The values of the redox potentials of the POM and bodipy are listed in Table 1. Notably, using the same electrolyte salt ($TBAPF_6$), the first two reduction processes are *ca.* 115 mV more negative for **TBA-K$_{Si}$[BOD]** in $CH_2Cl_2$ compared to MeCN, with the value in DMF being positioned in-between. A similar trend is observed with **TBA-D$_{Si}$[BOD]**, with a maximum variation of about 140 mV on the first wave and slightly more (160 mV) on the second between MeCN and $CH_2Cl_2$ solutions. Changing the nature of the electrolyte also has a notable impact with the first reduction of the Dawson-based hybrid wave being 230 mV more positive with $TMAClO_4$ than with $TBAPF_6$ in DMF and a change of up to 360 mV on the second reduction process.

**Table 1.** Half-wave potentials (*vs.* SCE, in V) and peak-to-peak separation (mV) of the redox processes for the reported hybrids.

| Hybrid | Solvent | Electrolyte | $[BOD]^+/[BOD]^a$ | $[BOD]/[BOD]^-$ | POM/POM+1e | POM+1e/POM+2e |
|---|---|---|---|---|---|---|
| **TBA-K$_{Si}$[BOD]** | $CH_2Cl_2$ | $TBAPF_6$ | 1.02 | -1.30 (80) | -0.45 (80) | -0.96 (70) |
| **TBA-K$_{Si}$[BOD]** | MeCN | $TBAPF_6$ | 1.01 | -1.18 (70) | -0.33 (70) | -0.85 (80) |
| **TBA-K$_{Si}$[BOD]** | DMF | $TBAPF_6$ | 1.03 | -1.10 (70) | -0.36 (70) | -0.95 (80) |
| **TBA-D$_{Si}$[BOD]** | $CH_2Cl_2$ | $TBAPF_6$ | 1.00 | -1.31 (100) | -0.71 (80) | -1.10 (80) |
| **TBA-D$_{Si}$[BOD]** | MeCN | $TBAPF_6$ | 0.99 | -1.20 (70) | -0.57 (70) | -0.94 (70) |
| **TBA-D$_{Si}$[BOD]** | DMF | $TBAPF_6$ | 1.03 | -1.10 (80) | -0.69 (70) | -1.10 (80) |
| **TBA-D$_{Si}$[BOD]** | DMF | $TEAClO_4$ | 0.97 | -1.17 (20) | -0.50 (80) | -0.93 (40) |
| **TBA-D$_{Si}$[BOD]** | DMF | $TMABF_4$ | 1.05 | -1.13 (70) | -0.46 (70) | -0.74 (70) |

[a] The standard potentials of irreversible processes were estimated by differential pulse voltammetry (Figures S7-S10).

Such changes of the redox properties due to various non-covalent interactions have been related to entropic effects associated with the significant modification of the solvation shells of the redox partners upon electron transfer.[14] The fact that redox potentials of POMs are considerably affected by the modification of the solvent and/or the associated counterions has often been reported[6a, 15] and outlines the importance of specific solvation with these multi-charged species. For instance, a correlation of the first one-electron reduction peak potential of POMs with the acceptor number of the solvent has been established.[16] The pronounced sensitivity of the redox properties of POMs to the solvent or its counterion will add further complexity to the photophysics. Not only will these modifications affect the reorganization energy upon photoinduced electron transfer, but also the thermodynamic parameters of these processes.

**Electronic absorption and photophysical properties**

The ground state absorption/emission of the Dawson-type hybrids are dominated by a $S_0$-$S_1$ transition at about 525-530 nm corresponding to the bodipy moieties, similarly to the Keggin analogue (Figures S11-12). The polyoxometalate framework absorbs into the UV-region and does not have an impact on the vibrational fine structure of the bodipy absorption bands, suggesting the two components are mostly electronically decoupled in the ground state. The molar extinction coefficient at the absorption maximum corresponding to the bodipy is approx. 140 000 $M^{-1}.cm^{-1}$. Table S1 summarizes the steady-state spectroscopic properties of **TBA-D$_{Si}$[BOD]** in different solvents. Results for the Keggin analogue have been previously reported.[9] As with **TBA-K$_{Si}$[BOD]**, the intrinsic fluorescence of the bodipy unit in the Dawson analogues is substantially quenched (by approx. 85%) in MeCN and $CH_2Cl_2$, which is consistent with charge separation competing effectively with radiative decay. A notable exception to this was observed when the hybrids were dissolved in DMF, in which case fluorescence was close to that of the parent bodipy (for **[BOD]** $\phi_F$ = 0.62, $\tau_{S1}$ = 4.4 ns). Transient absorption spectroscopy (TA) was then used to ascertain the electronic processes occurring following the excitation of the bodipy. The transient absorption spectra for **TBA-D$_{Si}$[BOD]** in $CH_2Cl_2$ are shown in Figure 1 and are consistent with data previously reported for **TBA-K$_{Si}$[BOD]**.[9] To extract the principle components, global analysis of the spectra was performed, in which the transients at all detection wavelengths are analyzed simultaneously with a single set of exponential functions.[17] At short delay times (0 to 300 ps) the transient absorption spectra of **TBA-D$_{Si}$[BOD]** contains a broad excited state absorption centered at 440 nm, a bleach at 520 nm, and a negative signal corresponding to stimulated emission between 550-700 nm, all consistent with the bodipy singlet-excited state.[9] This component decays with $\tau_1$ = 340 ps, as a second transient species with a sharp absorption at 405 nm grows in over the same timescale and decays with $\tau_2$ = 13 ns (Figure 1b). The absorption profile of the 405 nm species is consistent with the oxidized bodipy (note the absence of stimulated emission).[9] Furthermore, the transient also features a broad absorption extending past 700 nm, which follows the same kinetics as the oxidized bodipy, characteristic of the reduced POM (Figure S13).[2b, 7h] We therefore assign the second spectral component to the charge-separated state, [BOD$^+$-POM(+1 e$^-$)].

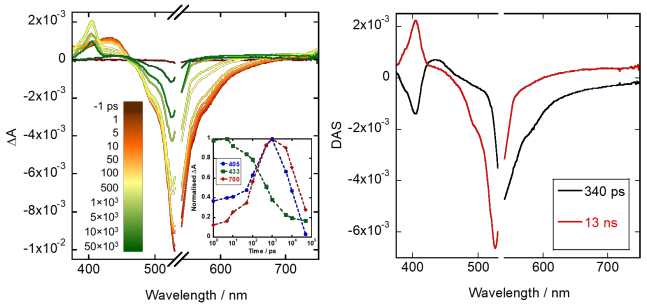


**Figure 1.** Transient absorption spectra of TBA-DSi[BOD] in CH2Cl2 following excitation at 540 nm (with a pump energy of 20 nJ and spot size of 150 μm): (a) transient absorption difference spectra at selected time delays after excitation; (b) decay associated difference spectra (DAS) from global analysis ($\tau_1$= ca. 340 ps and $\tau_2$ = ca. 13 ns).

A comparison of the lifetimes associated with the singlet excited state and charge-transfer excited state for **TBA-K$_{Si}$[BOD]**[9] and **TBA-D$_{Si}$[BOD]** in $CH_2Cl_2$ shows that charge separation and recombination of the Keggin-hybrid are considerably faster than those of the Dawson analogue (Table 2). This is consistent with our previous study of POM-iridium systems in which we observed that POMs with lower electron accepting properties displayed slower kinetics of charge separation (CS) / recombination (CR). The assumption is that CS occur in the Marcus normal region while the more exergonic CR occurs in the Marcus inverted region.[7h]

The transient absorption spectra of **TBA-K$_{Si}$[BOD]** and **TBA-D$_{Si}$[BOD]** were also recorded in more polar solvents such as MeCN ($\varepsilon$ = 37.5) and DMF ($\varepsilon$ = 36.7, Figures S14-S17, Table 2). As for $CH_2Cl_2$ ($\varepsilon$ = 8.93), the relaxation dynamics in MeCN can be accurately described using a two-component model, the first component corresponding to the formation of the charge separated state and the second to its decay.

**Table 2.** Time constant ($\tau$), for CS and CR of the POM-bodipy hybrids in $CH_2Cl_2$, MeCN and DMF at 298 K.

| Compound | Solvent | $\tau_{CS}$ (ps) | $\tau_{CR}$ (ns) | $\tau_{CR}$ / $\tau_{CS}$ |
|---|---|---|---|---|
| **TBA-K$_{Si}$[BOD]** | $CH_2Cl_2$ | 54 | 4.8 | 89 |
| **TBA-K$_{Si}$[BOD]** | MeCN | 38 | 1.3 | 34 |
| **TBA-K$_{Si}$[BOD]** | DMF | 2000 | 5.7 | 2.9 |
| **TBA-D$_{Si}$[BOD]** | $CH_2Cl_2$ | 340 | 13 | 38 |
| **TBA-D$_{Si}$[BOD]** | MeCN | 380 | 3.1 | 8.2 |
| **TBA-D$_{Si}$[BOD]** | DMF | 2400 | 10 | 10 |
| **TEA-D$_{Si}$[BOD]** | MeCN | 300 | 2.8 | 9.3 |
| **TEA-D$_{Si}$[BOD]** | DMF | 3000 | 6.7 | 2.2 |
| **TMA-D$_{Si}$[BOD]** | MeCN | 82 | 3.2 | 40 |
| **TMA-D$_{Si}$[BOD]** | DMF | 2100 | 5.3 | 2.5 |

The kinetics of charge separation are rather similar in these solvents, whereas the lifetime of the charge separated state is significantly shorter in a polar organic solvent like MeCN, than in $CH_2Cl_2$. In DMF, we observed that the formation of the charge-separated state is considerably slower (Figures S16, S17). For example, the excited and charge separation states for **TBA-$D_{Si}$[BOD]** decayed with $\tau$ = 2.4 ns and *ca.* 10 ns respectively. This is consistent with the high fluorescence quantum yield of this compound in this solvent (Table S1).

The effect of the counterion was also determined using transient absorption spectroscopy. This proved difficult to do in a systematic manner due to poor solubility in solvents other than DMF. In DMF, where all hybrids are soluble, the lifetime of the first component is shorter for **TMA-$D_{Si}$[BOD]** ($\tau$ = 2.0 ns) *vs.* **TEA-$D_{Si}$[BOD]** ($\tau$ = 3.0 ns), the TBA salt lying in-between ($\tau$ = 2.4 ns). In MeCN where the solubility of **TEA-$D_{Si}$[BOD]** and **TMA-$D_{Si}$[BOD]** is poor we still managed to extract kinetics for all systems. The transient spectra recorded in MeCN show that the charge separation is significantly accelerated going from **TBA-$D_{Si}$[BOD]** to **TMA-$D_{Si}$[BOD]**, **TEA-$D_{Si}$[BOD]** lying in-between, while the charge recombination occurs at a similar rate (Figures S15, S18 and S19). We did not succeed in solubilizing the TEA and TMA salt in $CH_2Cl_2$, yet we could solubilize a sample containing a mixed TMA/TBA salt (Figure S20). For this compound the charge injection was extremely fast ($\tau_{CS}$ = 4 ps), while charge separation remains relatively slow ($\tau_{CR}$ = 2.1 ns), yet as aggregation in this solvent cannot be excluded, the drastic acceleration of the charge separation can be attributed to other reasons than the sole effect of the counterion change.

**Theoretical calculations**

For a deeper understanding of the experimental results we applied computational methods on the target systems, namely density functional theory (DFT) and classical molecular dynamics (MD) (see the method in the SI file). Firstly, by means of MD simulations we analyzed the structure of solutions containing the **$D_{Si}$[BOD]** anion with different combinations of counter cations (TMA, TEA or TBA) and solvents (DMF, MeCN or $CH_2Cl_2$).

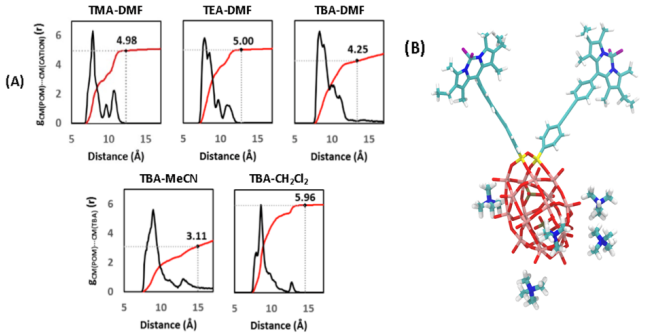


**Figure 2.** (a) RDFs ($g(r)$, black line), taking the center of mass of **$D_{Si}$[BOD]** as reference, of the counter cations for the systems DMF/X (X = TMA, TEA or TBA), $CH_2Cl_2$/TBA and MeCN/TBA. The integration of $g(r)$ (red line) and the coordination number shown indicate the number of species on average at a given distance from the reference. Data from the last 10 ns of each MD trajectory. (b) Snapshot of the simulation in DMF showing a highly representative interaction mode between the hybrid-POM and five TMA cations (the 6$^{th}$ cation is located in the bulk solution).

The results, shown in Figure 2, compare the radial distribution functions (RDFs) obtained. In DMF, the first peaks in the RDFs are found at 7.85 Å for TMA and TEA, a value that increases to 8.45 Å for TBA, the bulkiest cation of the series. In line with this, the computed coordination number for TBA is $N$ = 4.25 and $N$ = 5.0 for TEA and TMA respectively. Such a cation distribution around **$D_{Si}$[BOD]** is consistent with the interaction energies shown in Figure S21, revealing that the POM–cation interaction is significantly smaller for TBA (–419 kJ.mol$^{-1}$) vs –550 kJ.mol$^{-1}$ for TMA. The previous fact is reinforced by the high TBA-DMF affinity, -1229 kJ.mol$^{-1}$ (–219 kJ.mol$^{-1}$ per TBA unit), much larger than for the other cation-DMF pairs. Similar POM-cations analysis have been reported previously.[18] Interestingly, no cation was found near the organic part of the **$D_{Si}$[BOD]** system in our simulations, but mostly in the bulk of the solution or surrounding the negatively charged Dawson framework of **$D_{Si}$[BOD]**, as shown in Figure 2b. We have also evaluated the effect of the solvent by analyzing the distribution of TBA in $CH_2Cl_2$ and MeCN. The TBA coordinates poorly to the POM-hybrid ($N$ = 3.11) in MeCN as solvent. This trend is explained by the high POM-MeCN (Figure S21) and TBA-MeCN affinities, which result in a low POM-TBA interaction (–261 kJ.mol$^{-1}$). This is in agreement with the important discrepancy in the diffusion coefficients between hybrid POMs and their TBA cations that has been observed by DOSY NMR in this solvent.[19] At the opposite end, when the solvent is $CH_2Cl_2$, the POM-solvent and TBA-solvent pairs show poor affinities. Concomitantly, the POM-TBA interaction is maximal (–655 kJ.mol$^{-1}$) and $N \approx 6$. In comparison, the DMF case is located in-between the previous two in terms of POM-TBA coordination.

The electronic structure of **$D_{Si}$[BOD]** and its redox properties under the influence of the different solvents and counterions was computed with single point DFT calculations taking five random structures (hybrid-POM + counterions) of each MD trajectory. As shown in Table S2, the LUMO energy ($E_{LUMO}$) of the cation-hybrid system depends largely on the solvent and the number of counterions ($N$) in contact with the POM. The relevance of the solvent is clearly visible in the values of the three first entries. Hence, whereas $E_{LUMO}$ is –4.117 eV for the TBA-$CH_2Cl_2$ system, in MeCN the corresponding value decreases to –4.312 eV. Consequently, a change in the redox potential of about 195 mV is expected, not far from the 140 mV observed. $E_{LUMO}$ depends also on the pairing between the POM and the counterions. The higher the ion pairing, the deeper the LUMO. In DMF, the highest LUMO is found with TBA (–4.284 eV) and the lowest one with TMA (–4.414 eV), the latter system featuring the highest ion pairing. Thus, the combination of MD simulations with molecular orbital analysis computed at the DFT/BP86 level with a Slater TZP basis set allows a reasonable match with the redox properties of the **$D_{Si}$[BOD]** anion in different solvents. Similar results were found with the PBE functional (Table S3). Although theoretical studies on the redox properties of POMs have already been reported,[20] to our knowledge, this is the first case in which a systematic analysis on the influence of cations on the reduction potentials of a POM has been performed.

State-of-the-art computational methods can also be very helpful in the understanding of the kinetics of electron transfer (ET) processes in complex systems such as hybrid POMs. Theoretical estimation of the reorganization energy, $\lambda$, can indeed allow evaluating the roles played by the solvent and the

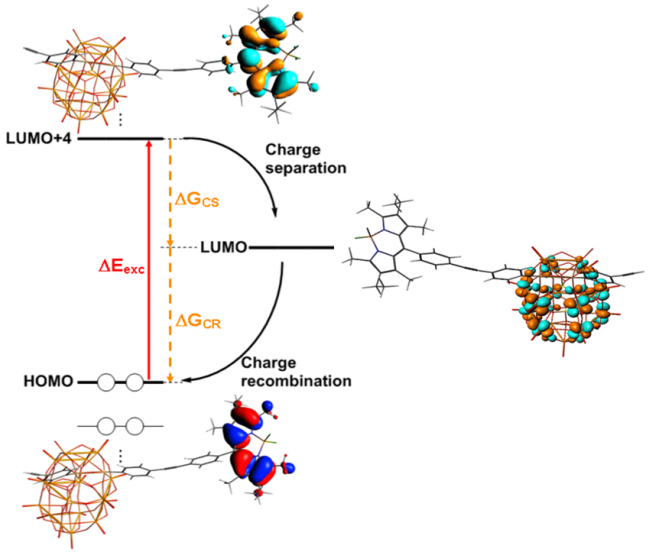


**Figure 3.** Schematic view of the processes taking place in **$D_{Si}$[BOD]** upon irradiation.

POM framework in the kinetics of ET processes. In Figure 3, the vertical red arrow represents the HOMO (π) → LUMO+4 (π) (lowest unoccupied orbital localized on the bodipy) electron transition dominating the photoexcitation of the system under visible light. It was determined with time-dependent DFT (TD-DFT) (Figure S22) with an energy of 2.52 eV, *ca.* 0.2 eV higher compared to the experimental value.

To investigate how the kinetics of CS and CR depend on the medium containing the POM-hybrid system, some of us used a recently proposed strategy to determine the associated reorganization energies, λ and free energy barriers, $\Delta G^{\neq}$.[21] According to Marcus theory, the rate constant for an electron transfer process of a supramolecular system in the nonadiabatic limit (*i.e.* when its different elements are poorly electronically coupled) can be expressed by equations (1).[22],[23] In the current case, considering the electron decoupling between the organic and inorganic moieties,[12] it is likely that the electron transfer would occur through space.

$$k_{ET} = \nu \exp\left(\frac{-\Delta G^{\neq}}{k_B T}\right) \qquad \Delta G^{\neq} = \frac{(\lambda + \Delta G^{\circ})^2}{4\lambda} \qquad (1)$$

Here ν is an electronic factor that depends on the overlap between the electronic wavefunctions of the donor and acceptor groups, $\Delta G^{\circ}$ is the standard free energy change of the reaction, and λ is the reorganization energy. In this approach, the medium (solvent+counterions) is implicitly included in the DFT calculations.[24] Table 3 and Table S4 list the values computed for the systems based on Keggin and Dawson frameworks in $CH_2Cl_2$, MeCN and DMF. In the initial models of the Marcus theory, the total λ was estimated from separate contributions for the electron donor, the acceptor and the medium.[22-23] In our system, assuming that BOD and POM are two distinct fragments acting as electron donor and acceptor, we compute $\lambda = \lambda_{BOD} + \lambda_{POM}$ alternatively, each being the joint contribution donor+medium or acceptor+medium. The surroundings of **$D_{Si}$[BOD]** are represented by a set of point charges in our DFT setup, thus the calculation of $\lambda_{POM}$ (and $\lambda_{BOD}$) does not account for the effect of the cation size. However, we know from MD results that $\lambda_{BOD}$ must not depend on the cation nature directly, as cations do not enclose the BOD group. This is at variance to the Dawson framework and $\lambda_{POM}$. As shown in Table 3 and Table S4, the reorganization energies for the **$D_{Si}$[BOD]** anion were estimated to be 0.94 eV in $CH_2Cl_2$, 1.07 eV in DMF and 1.19 eV in MeCN with rather similar contributions from BOD and POM moieties. The driving force for **TBA-$D_{Si}$[BOD]** of the charge separation is estimated to be –0.74, -0.96 and –1.01 eV in $CH_2Cl_2$, DMF and MeCN respectively. $\Delta G_{CS}$ can also be estimated from the Rehm-Weller eq. 2.[25]

$$\Delta G_{CS} = E(BOD/BOD^{+}) - E(POM/POM^{-}) - E_{00} + w_{el} \qquad (2)$$

The Coulombic interaction ($w_{el}$) between the positive and negative charges was evaluated from the optimized structure of **TBA-$D_{Si}$[BOD]**. Using the values $R_{BOD+\text{-}POM-}$ = 19.9 Å, the work term is evaluated to be 0.08 eV in $CH_2Cl_2$ and 0.02 eV in MeCN and DMF (neglecting the distribution of some TBA cations in the medium). The theoretical values of $\Delta G^{\circ}$ (*i.e.* $\Delta G_{CS}$) are slightly more negative albeit in good agreement with the experimental ones.

Equivalent MD simulations were carried out for the Keggin-based system **$K_{Si}$[BOD]** (Figure S23) to analyze the distribution of counter cations around the hybrid. This followed the procedure described above for **$D_{Si}$[BOD]** to determine the stabilization of the Keggin fragment and their frontier orbitals in $CH_2Cl_2$ and MeCN. From Table 3 it stands out that the LUMO for the Keggin system is 0.3–0.5 eV (depending on the solvent) deeper than that of **$D_{Si}$[BOD]** in agreement with the electrochemical study. The evaluation of the calculated reorganization energy shows that the contribution of the Keggin is slightly higher than that of the Dawson in both solvents. Furthermore for **$K_{Si}$[BOD]** the driving force is very close to the reorganization energy, which is in agreement with the very fast electron transfer in this compound. A correlation between the computed activation energy barriers (using the experimental free energies) and the electron transfer rates is observed for **TBA-$K_{Si}$[BOD]** and **TBA-$D_{Si}$[BOD]** in $CH_2Cl_2$ and MeCN (Figure S24). Eventhough this correlation is simplistic since it implies that the electronic factor ν is the same for all systems, its observation suggests that the computed λ values are reasonably good. Note that, for CS, as the driving force is close (in absolute value) to the reorganization energy, slight uncertainties on the estimation of the reorganization energy have a drastic consequence on the free activation barrier, which is not the case for charge recombination that occurs deep in the Marcus inverted region. This explains the better correlation for CR than for CS. CS and CR times cannot be directly compared with the sole values of the energy barriers since the electronic factor ν is significantly different in the charge separation and in the charge recombination. Indeed, it depends on the overlap between LUMO+4 (donor) and LUMO (acceptor) for the charge separation and the overlap between LUMO (donor) and HOMO (acceptor) for the charge recombination. Interestingly the LUMO + 4 has an important contribution at the meso position connecting the bodipy to the POM while this position corresponds to a node in the HOMO (Figure 3). This shows that the electronic factor for the charge separation is higher than that of the charge recombination in agreement with the experimental observation.

**Table 3.** Selected parameters relevant for the charge separation and recombination steps for **TBA-D$_{Si}$[BOD]** and **TBA-K$_{Si}$[BOD]** systems in $CH_2Cl_2$, MeCN and DMF.

| Compound / solvent | LUMO / eV | λ / eV | $-\Delta G_{CS}$ / eV DFT[a] | Expt | $\Delta G_{CS}^{\neq}$ [b] / kJ.mol$^{-1}$ | $\tau_{CS}$ / ps | $-\Delta G_{CR}$ / eV DFT[c] | Expt | $\Delta G_{CR}^{\neq}$ [b] / kJ.mol$^{-1}$ | $\tau_{CR}$ / ns |
|---|---|---|---|---|---|---|---|---|---|---|
| **TBA-D$_{Si}$[BOD]** / $CH_2Cl_2$ | –4.117 | 0.94 | 0.74 | 0.70 | 1.46 (1.00) | 340 | 1.78 | 1.63 | 12.3 (18.2) | 13 |
| **TBA-D$_{Si}$[BOD]** / MeCN | –4.312 | 1.19 | 1.01 | 0.80 | 3.07 (0.62) | 380 | 1.51 | 1.54 | 2.50 (2.05) | 3.1 |
| **TBA-D$_{Si}$[BOD]** / DMF | –4.284 | 1.07 | 0.96 | 0.62 | 4.58 (0.27) | 2400 | 1.56 | 1.70 | 8.92 (5.38) | 10 |
| **TBA-K$_{Si}$[BOD]** / $CH_2Cl_2$ | –4.641 | 0.99 | 1.20 | 0.94 | 0.06 (1.15) | 54 | 1.32 | 1.39 | 3.96 (2.64) | 4.8 |
| **TBA-K$_{Si}$[BOD]** / MeCN | –4.677 | 1.24 | 1.28 | 1.02 | 0.94 (0.03) | 38 | 1.24 | 1.32 | 0.13 (0.00) | 1.3 |
| **TBA-K$_{Si}$[BOD]** / DMF | –4.670 | 1.11 | 1.26 | 0.95 | 0.58 (0.47) | 2000 | 1.26 | 1.39 | 1.65 (0.46) | 5.7 |

[a] Estimate of $\Delta G_{CR}$ obtained as difference between the energy of the excited electron and the LUMO of the molecule. [b] Free energy barriers calculated with eq. 2. In parentheses, free energy barriers estimated using the computed values for $\Delta G_{CS}$. [c] Estimate of $\Delta G_{CR}$ obtained as difference between LUMO and the HOMO energies of the molecule, which are localized on the POM and BOD, respectively.

## Discussion

Theoretical calculations clearly show that the respective solvation energy of the POM, the counterion and POM-cation affinity cause a considerable modification of the redox potentials depending on the nature of the solvent and the associated counterion. This study also demonstrates that the calculated reorganization energy is significantly higher in MeCN than in $CH_2Cl_2$ owing to a difference in polarity. Furthermore, it shows that Keggin-type POMs have higher reorganization energies than Dawson analogues. Finally, we showed that with similar free energy barrier the CS is considerably faster than the CR owing to a difference in the electronic contribution at the bodipy meso position in the ground state and the bodipy excited state, which provides directionality in the photoinduced electron transfers. From the theoretical study and electrochemistry, we observed that the hybrids displayed more negative reduction potential in $CH_2Cl_2$. Consequently the driving force for the CS is more favorable in MeCN and in DMF than in $CH_2Cl_2$. The fact that the kinetics of charge separation are similar in $CH_2Cl_2$ and MeCN suggests that the loss in the driving force (*ca.* 0.10 eV for **TBA-K$_{Si}$[BOD]** and **TBA-D$_{Si}$[BOD]**) is compensated by a lower reorganization energy. The difference in the calculated reorganization energy in $CH_2Cl_2$ and in MeCN is slightly more significant (0.25 eV) and possibly reflects a minor overestimation in MeCN. The lifetime of the charge separated state is 3 to 4 times higher in $CH_2Cl_2$ than in MeCN. Indeed, for CR, the change from MeCN to $CH_2Cl_2$, both lowers the reorganization energy and increases the driving force of the CR (Figure 4). Considering that the CR occurs in the Marcus inverted region, both effects will tend to increase the activation energy and hence increase the lifetime of the charge-separated state.

The slow kinetics of CS in DMF for all hybrids is still surprising. Indeed, the redox potentials of the hybrids in DMF are in-between those in $CH_2Cl_2$ and MeCN. Furthermore the calculated reorganization energy in this solvent also falls in-between those calculated in MeCN and $CH_2Cl_2$. Based on these features, it would have been expected that the kinetics of the photoinduced electron transfer would be similar in DMF to that in MeCN and/or $CH_2Cl_2$. As in DMF, the CR is also slow (Table 3), an explanation could be that the electronic factor ν would be unexpectedly low in this solvent. The origin of the slow electron transfer kinetics in DMF is probably related to the higher viscosity of this solvent (0.80 cP at 25°C) compared to that of MeCN (0.34 cP ar 25°C) or $CH_2Cl_2$ (0.41 cP at 25°C) and the important solvation energy of the TBA cations in this solvent (Figure S21). It is then very likely that in DMF the exchange of the TBA cations would be very slow. The role of solvation dynamics (and notably the viscosity of the solvent) on photoinduced elecron transfer has indeed been clearly identified in several studies.[26] In the present case, theoretical calculations have shown that in DMF some of the TBA cations are located in the bulk solvent. In this solvent, the slow electron transfer is then consistent with a mechanism in which the

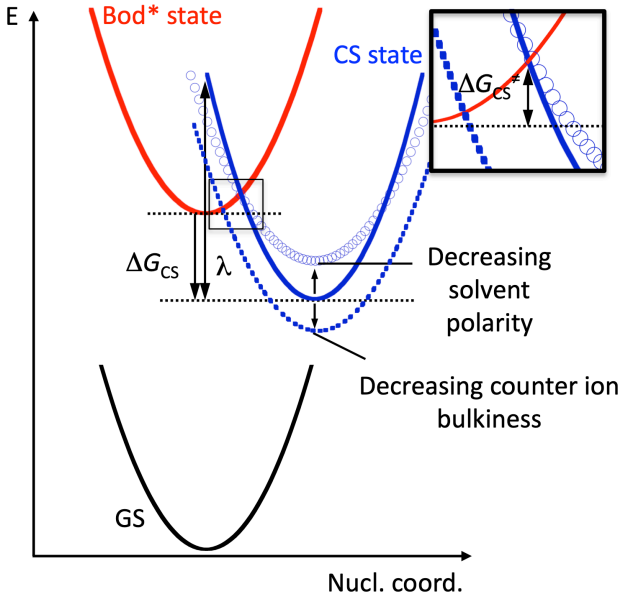


**Figure 4.** Profile of the potential energy curves of the photoinduced electron transfer reaction. The red, blue and black curves correspond to the bodipy centered excited state, the charge separated state and ground state respectively. The blue dotted curve and the circles curves correspond to the effects of decreasing counterion bulkiness (from TBA to TMA) or decreasing the solvent polarity (from MeCN to $CH_2Cl_2$) respectively. The inset shows a detail of the crossing of the BOD* and charge-separated states.

electron transfer step would be gated by the slow counterion rearrangement (*i.e.* change of the coordination number for permitting the electron transfer), which is not the case in $CH_2Cl_2$ in which all counterions are located at the vicinity of the POM or in MeCN in which the counterion exchange is much faster (lower viscosity and lower solvation of the TBA cations). The nature of the POM counterion also has an important effect on the photophysical properties of the photosensitized POM-based hybrids. Indeed not only does the counterion affect the driving force by modifying the redox potentials of the POM (as evidenced by electrochemistry and theoretical calculations), but it should also modify the reorganization energy, even though the cation size effect was not considered in the calculation of $\lambda$. The effect is rather weak in DMF but much greater in MeCN. This is exemplified in the case of the mixed cation **TMA,TBA-$D_{Si}$[BOD]** for which the CS is accelerated by two orders of magnitude in $CH_2Cl_2$ compared to **TBA-$D_{Si}$[BOD]**. The Dawson hybrid **TMA,TBA-$D_{Si}$[BOD]** (albeit poorly soluble) in $CH_2Cl_2$ hence constitutes the most effective system displaying ultra fast CS and long-lived charge separated state.

## Conclusion

A series of Dawson-type POM-bodipy hybrids were synthesized in which the counterion was systematically varied in terms of bulkiness through TMA, TEA and TBA. The electrochemical and photophysical properties of these systems were examined in different solvents in order to evaluate the effect of both counterion and solvent on photoinduced electron transfer. Although poor solubility of certain hybrids in some solvents was a challenge, it was possible to determine that an increase in solvent polarity led to a decrease in the lifetime of the charge separated state. Similarly decreasing the cation bulkiness leads to an acceleration of the CS, the lifetime of the charge separated state remaining relatively unaffected. This is rationalized by Marcus theory, where changes in reorganization energy compensate for the clear changes in thermodynamic driving force as observed from electrochemical measurements. Theoretical investigation corroborated these observations. This work, which combined DFT and molecular dynamics simulation methods, constitutes the first study on the influence of cations on the reduction potentials of a POM. It showed that the solvation energy of the POM and the counterion and POM-cation affinity are at the origin of a considerable modification of the redox potentials according to the nature of the solvent and the associated counterion and also suggested that the solvation dynamics can drastically affect the kinetics of photoinduced electron transfer. This study also allowed an evaluation of the reorganization energy of the hybrids, which were in good agreement with those expected from the photophysical study. Finally it was shown that the functionalization of the bodipy at the meso position provides directionality in the photoinduced electron transfers. Our findings show that careful control of the environment around the POM can have a major impact on the dynamics of photoinduced electron transfer, and that a quantitative survey may optimize the intramolecular process.

## Acknowledgements

EAG, FAB and JK thank The North East Centre for Energy Materials EP/R021503/1, ERC starting grant, p-TYPE 715354, LaserLab Europe LLC002553, STFC for access to the CLF ULTRA facility at the Rutherford Appleton Laboratories, the EPSRC and Newcastle University for a studentship for FAB (EPJ5002881). JMP thanks Spanish Ministry of Science (grant CTQ2017-87269-P), the Generalitat de Catalunya (grant 2017SGR629) and the URV for support. JMP also thanks the ICREA foundation for an ICREA ACADEMIA award. GI, AP, SB and YB M'B thank the French National Research Agency for Grant ANR PhotoCarb (ANR-16-CE05-0025- 03). TP and PC acknowledge financial support from Swedish Energy Agency and the Swedish Research Council.

**Keywords:** Photoinduced electron transfer • Polyoxometalate-based hybrids • DFT/ molecular dynamic (MD) simulations • Transient absorption spectroscopy • Non-covalent interactions.

## References

[1] a) Y. F. Song, R. Tsunashima, *Chem. Soc. Rev.* **2012**, *41*, 7384-7402; b) H. N. Miras, J. Yan, D. L. Long, L. Cronin, *Chem. Soc. Rev.* **2012**, *41*, 7403-7430; c) A. Proust, B. Matt, R. Villanneau, G. Guillemot, P. Gouzerh, G. Izzet, *Chem. Soc. Rev.* **2012**, *41*, 7605-7622.

[2] a) J. J. Walsh, A. M. Bond, R. J. Forster, T. E. Keyes, *Coord. Chem. Rev.* **2016**, *306*, 217-234; b) B. Matt, J. Fize, J. Moussa, H. Amouri, A. Pereira, V. Artero, G. Izzet, A. Proust, *Energy Environ. Sci.* **2013**, *6*, 1504-1508; c) K. Nakanishi, G. J. T. Cooper, L. J. Points, L. G. Bloor, M. Ohba, L. Cronin, *Angew. Chem., Int. Ed.* **2018**, *57*, 13066-13070.

[3] L. Chen, W. L. Chen, X. L. Wang, Y. G. Li, Z. M. Su, E. B. Wang, *Chem. Soc. Rev.* **2019**, *48*, 260-284.

[4] a) P. Yang, W. L. Zhao, A. Shkurenko, Y. Belmabkhout, M. Eddaoudi, X. C. Dong, H. N. Alshareef, N. M. Khashab, *J. Am. Chem. Soc.* **2019**, *141*, 1847-1851; b) Y. C. Ji, L. J. Huang, J. Hu, C. Streb, Y. F. Song, *Energy Environ. Sci.* **2015**, *8*, 776-789; c) J. Hu, Y. C. Ji, W. Chen, C. Streb, Y. F. Song, *Energy Environ. Sci.* **2016**, *9*, 1095-1101; d) N. Kawasaki, H. Wang, R. Nakanishi, S. Hamanaka, R. Kitaura, H. Shinohara, T. Yokoyama, H. Yoshikawa, K. Awaga, *Angew. Chem., Int. Ed.* **2011**, *50*, 3471-3474; e) Y. Nishimoto, D. Yokogawa, H. Yoshikawa, K. Awaga, S. Irle, *J. Am. Chem. Soc.* **2014**, *136*, 9042-9052; f) M. Bonchio, Z. Syrgiannis, M. Burian, N. Marino, E. Pizzolato, K. Dirian, F. Rigodanza, G. A. Volpato, G. La Ganga, N. Demitri, S. Berardi, H. Amenitsch, D. M. Guldi, S. Caramori, C. A. Bignozzi, A. Sartorel, M. Prato, *Nat. Commun.* **2019**, *11*, 495-495.

[5] A. Misra, K. Kozma, C. Streb, M. Nyman, *Angew. Chem., Int. Ed.* **2020**, *59*, 596-612.

[6] a) M. Sadakane, E. Steckhan, *Chem. Rev.* **1998**, *98*, 219-237; b) I. A. Weinstock, R. E. Schreiber, R. Neumann, *Chem. Rev.* **2018**, *118*, 2680-2717.

[7] a) A. Harriman, K. J. Elliott, M. A. H. Alamiry, L. Le Pleux, M. Severac, Y. Pellegrin, E. Blart, C. Fosse, C. Cannizzo, C. R. Mayer, F. Odobel, *J. Phys. Chem. C* **2009**, *113*, 5834-5842; b) F. Odobel, M. Severac, Y. Pellegrin, E. Blart, C. Fosse, C. Cannizzo, C. R. Mayer, K. J. Eliott, A. Harriman, *Chem. Eur. J.* **2009**, *15*, 3130-3138; c) M. K. Seery, L. Guerin, R. J. Forster, E. Gicquel, V. Hultgren, A. M. Bond, A. G. Wedd, T. E. Keyes, *J. Phys. Chem. A* **2004**, *108*, 7399-7405; d) C. Allain, D. Schaming, N. Karakostas, M. Erard, J. P. Gisselbrecht, S. Sorgues, I. Lampre, L. Ruhlmann, B. Hasenknopf, *Dalton Trans.* **2013**, *42*, 2745-2754; e) S. Schonweiz, S. A. Rommel, J. Kubel, M. Micheel, B. Dietzek, S. Rau, C. Streb, *Chem. Eur. J.* **2016**, *22*, 12002-12005; f) Y. Luo, M. Wachtler, K. Barthelmes, A. Winter, U. S. Schubert, B. Dietzek, *Chem. Commun.* **2018**, *54*, 2970-2973; g) B. Matt, C. Coudret, C. Viala, D. Jouvenot, F. Loiseau, G. Izzet, A. Proust, *Inorg. Chem.* **2011**, *50*, 7761-7768; h) B. Matt, X. Xiang, A. L. Kaledin, N. N. Han, J. Moussa, H. Amouri, S. Alves, C. L. Hill, T. Q. Lian, D. G. Musaev, G. Izzet, A. Proust, *Chem.*

*Sci.* **2013**, *4*, 1737-1745; i) C. C. Zhao, Z. Q. Huang, W. Rodriguez-Cordoba, C. S. Kambara, K. P. O'Halloran, K. I. Hardcastle, D. G. Musaev, T. Q. Lian, C. L. Hill, *J. Am. Chem. Soc.* **2011**, *133*, 20134-20137.

[8] M. R. Wasielewski, *Chem. Rev.* **1992**, *92*, 435-461.

[9] F. A. Black, A. Jacquart, G. Toupalas, S. Alves, A. Proust, I. P. Clark, E. A. Gibson, G. Izzet, *Chem. Sci.* **2018**, *9*, 5578-5584.

[10] Acronyms used for the hybrid POMs: K and D refer to Keggin- and Dawson-types anion, Si as subscript relates to the primary functionalization and the term in brackets corresponds to the remote organic moieties.

[11] a) V. Duffort, R. Thouvenot, C. Afonso, G. Izzet, A. Proust, *Chem. Commun.* **2009**, 6062-6064; b) B. Matt, S. Renaudineau, L. M. Chamoreau, C. Afonso, G. Izzet, A. Proust, *J. Org. Chem.* **2011**, *76*, 3107-3112.

[12] G. Izzet, F. Volatron, A. Proust, *Chem. Rec.* **2017**, *17*, 250-266.

[13] N. Elgrishi, K. J. Rountree, B. D. McCarthy, E. S. Rountree, T. T. Eisenhart, J. L. Dempsey, *J. Chem. Educ.* **2018**, *95*, 197-206.

[14] a) B. T. Huang, S. Muy, S. T. Feng, Y. Katayama, Y. C. Lu, G. Chen, Y. Shao-Horn, *Phys. Chem. Chem. Phys.* **2018**, *20*, 15680-15686; b) H. Svith, H. Jensen, J. Almstedt, P. Andersson, T. Lundback, K. Daasbjerg, M. Jonsson, *J. Phys. Chem. A* **2004**, *108*, 4805-4811.

[15] a) S. Himeno, M. Takamoto, R. Santo, A. Ichimura, *Bull. Chem. Soc. Jpn.* **2005**, *78*, 95-100; b) S. X. Guo, A. W. A. Mariotti, C. Schlipf, A. M. Bond, A. G. Wedd, *J. Electroanal. Chem.* **2006**, *591*, 7-18; c) V. A. Grigoriev, D. Cheng, C. L. Hill, I. A. Weinstock, *J. Am. Chem. Soc.* **2001**, *123*, 5292-5307; d) S. X. Guo, A. W. A. Mariotti, C. Schlipf, A. M. Bond, A. G. Wedd, *Inorg. Chem.* **2006**, *45*, 8563-8574.

[16] B. Keita, D. Bouaziz, L. Nadjo, *J. Electrochem. Soc.* **1988**, *135*, 87-91.

[17] C. Slavov, H. Hartmann, J. Wachtveitl, *Anal. Chem.* **2015**, *87*, 2328-2336.

[18] E. Nikoloudakis, K. Karikis, M. Laurans, C. Kokotidou, A. Sole-Daura, J. J. Carbo, A. Charisiadis, G. Charalambidis, G. Izzet, A. Mitraki, A. M. Douvas, J. M. Poblet, A. Proust, A. G. Coutsolelos, *Dalton Trans.* **2018**, *47*, 6304-6313.

[19] a) K. Sakanoue, M. Motoda, M. Sugimoto, S. Sakaki, *J. Phys. Chem. A* **1999**, *103*, 5551-5556; b) V. Vaissier, P. Barnes, J. Kirkpatrick, J. Nelson, *Phys. Chem. Chem. Phys.* **2013**, *15*, 4804-4814.

[20] a) X. Lopez, J. M. Poblet, *Inorg. Chem.* **2004**, *43*, 6863-6865; b) I. M. Mbomekalle, X. Lopez, J. M. Poblet, F. Secheresse, B. Keita, L. Nadjo, *Inorg. Chem.* **2010**, *49*, 7001-7006.

[21] a) P. Song, Y. Z. Li, F. C. Ma, T. Pullerits, M. T. Sun, *J. Phys. Chem. C* **2013**, *117*, 15879-15889; b) Y. J. Hu, A. Sole-Daura, Y. R. Yao, X. C. Liu, S. J. Liu, A. Yu, P. Peng, J. M. Poblet, A. Rodriguez-Fortea, L. Echegoyen, F. F. Li, *Chem. Eur. J.* **2020**, *26*, 1748-1753.

[22] R. A. Marcus, *Annu. Rev. Phys. Chem.* **1964**, *15*, 155-196.

[23] P. Ceroni, V. Balzani, in *The exploration of supramolecular systems and nanostructures by photochemical techniques* (Ed.: P. Ceroni), Springer, New York, **2011**.

[24] a) X. Lopez, J. J. Carbo, C. Bo, J. M. Poblet, *Chem. Soc. Rev.* **2012**, *41*, 7537-7571; b) X. Lopez, J. A. Fernandez, J. M. Poblet, *Dalton Trans.* **2006**, 1162-1167.

[25] a) D. Rehm, A. Weller, *Ber. Bunsen-Ges. Phys. Chem.* **1969**, *73*, 834-839; b) D. Rehm, A. Weller, *Isr. J. Chem.* **1970**, *8*, 259-271.

[26] a) R. A. Marcus, *J. Phys. Chem. B* **1998**, *102*, 10071-10077; b) N. Bodappa, Y. C. Fu, P. Broekmann, J. Furrer, K. Zick, S. Vesztergom, H. Tahara, T. Sagara, *Electrochim. Acta* **2019**, *320*; c) L. Qin, N. M. Kostic, *Biochemistry* **1994**, *33*, 12592-12599; d) J. S. Zhou, N. M. Kostic, *J. Am. Chem. Soc.* **1993**, *115*, 10796-10804; e) X. Zhang, J. Leddy, A. J. Bard, *J. Am. Chem. Soc.* **1985**, *107*, 3719-3721.